Available online at www.sciencedirect.com
ScienceDirect
Journal of Sound and Vibration 302 (2007) 332–349
JOURNAL OF SOUND AND VIBRATION
www.elsevier.com/locate/jsvi

Vibrational power flow analysis of thin cylindrical shell with a circumferential surface crack

X. Zhu, T.Y. Li*, Y. Zhao, J. Yan

Department of Naval Architecture & Ocean Engineering, Huazhong University of Science & Technology, Wuhan 430074, PR China

Received 12 April 2006; received in revised form 27 July 2006; accepted 3 December 2006
Available online 19 January 2007

Abstract

In the view of structure-borne sound, the structural wave and power flow characteristics of infinite thin cylindrical in vacuo shell with a circumferential surface crack are investigated. In this paper, the equivalent distributed line spring is designed to model the surface crack in the shell. The local compliance matrix due to the presence of the crack is deduced from fracture mechanics and three modes of the crack stress intensity factors and their coupling are considered in the local compliance matrix. The vibration of the thin shell is described by the Flügge shell equations. Under the excitation of radial harmonic line force, the input power flow and transmitted power flow of uncracked and cracked shells are obtained. The results show that the vibrational power flow of cracked shell changes substantially due to the presence of crack, and the change is strongly related to the depth and location of crack. Contours of input power flow at different frequencies are constructed to identify the location and depth of the crack. It is revealed that the power flow in the cylindrical shell structures can be used as an alternative defect information carrier. This research provides theoretical basis for the crack detection by measuring the vibrational power flow in cracked shell structures.

1. Introduction

Cracks are often found in the engineering structures due to different causes, which present a serious threat to the performance of structures. For this reason, early detection and localization of the cracks have been the subject of many investigators for decades and a number of damage-detection methods have been developed. The conventional non-destructive evaluation methods, such as ultrasonic testing, X-ray, magnetic field methods, etc. are usually costly and time consuming for the large-scale structure. Generally, a crack in a structure introduces a local flexibility which usually changes the dynamic behavior of the structure, and the usage of such changes could be a possible way to detect the crack. Therefore, the vibration-based crack identification methods are utilized widely in recent years. Based on this principle, many crack detection methods have been developed: frequency change, mode shape change, flexibility change, impedance method, method based on wavelet, neural network method, etc. Doebling et al. [1] presented a review of the state of the art of vibration-based damage detection methods.

*Corresponding author.
E-mail address: ltyz801@tom.com (T.Y. Li).

0022-460X/$ - see front matter © 2006 Published by Elsevier Ltd.
doi:10.1016/j.jsv.2006.12.001

In recent literatures, most of the researches for crack detection were concentrated on the simple beam structures and plate structures [2]. In the beam or plate structures, many methods are used to model the crack, such as the short beam model, finite element method and rotational spring model, and so on. Gounaris and Dimarogonas [3] developed a finite element for a cracked prismatic beam for structural analysis based on the compliance matrix for the crack. Chaudhari and Maiti [4] modeled the crack section by a rotational spring to analyze the transverse vibrations of a geometrically segmented slender beam and identify the crack in the beam. The line spring model was also used to determine the local flexibility in the research of the cracked plate structures [5–7]. From kinds of literatures it can be found that the local spring model is by far the most commonly used model in dynamic analysis of cracked beams.

However, the damage detection researches on shell structures received scant attention from literatures, perhaps due to the complexity of the cylindrical shell structures. Srinivasan and Kot [8] used the modal strain energy as the indicator of damage in a cylindrical shell and proposed the damage index algorithm to detect the damage. Nikpour [9] analyzed the influence of a circumferential crack upon the vibration characteristics of a thin laminated anisotropic cylindrical shell and the case of axisymmetrical vibration demonstrated the modal frequency technique to estimate the position and depth of the crack. Marwala [10] presented a committee of neural networks technique, which employed frequency response functions, modal properties (natural frequencies and mode shapes), and wavelet transform data simultaneously to identify four types of faults in a cylindrical shell and this committee approach gave results that generally have a lower mean square error (MSE) than the average MSE of the individual methods. Roytman and Titova [11] provided an analytical approach to determining the dynamic characteristics of a cylindrical shell with closing cracks, and the cycle of vibrations was assumed to be subdivided into two parts and the problem was solved in a piecewise linear with different frequencies and amplitudes at each vibrations cycle interval. From the above discussions, it is apparent that investigations on crack detection of shell structures are not enough and some new methods should be proposed to detect the crack in the cylindrical shell structures.

In recent years, the structure-borne sound analysis and control of flexible structures such as cabins of marine-structures and aeronautical crafts are becoming an important topic. The usage of vibrational power flow in the problem of this type is very valuable. Generally, the vibration of a structure can be regarded as a typical example of structural wave propagation. The presence of the crack in the structure will in some way change the motion of the wave. Consequently, the changes of the wave will in turn influence the power flow characteristics in the structure. Based on this, the research on the power flow characteristics of the cracked structures will be of great value for crack detection. Li et al. [12,13] firstly researched the power flow of the cracked periodic beam structures and cracked infinite beam structures. The relations between the vibrational power flow and the characteristics of the crack (location and depth) were obtained to detect the crack. Li et al. [14] again investigated the power flow characteristics of the circular plate structure with peripheral surface crack.

The objective of this paper is to investigate the power flow characteristics of the infinite thin cylindrical in vacuo shell with a circumferential surface crack The part-through cracked section is represented as a continuous line spring. In consideration of the three modes of stress intensity factors, the local compliance matrix is obtained from fracture mechanics to construct the boundary condition in the vicinity of the crack. Using the Flügge shell equations, the wave propagation and power flow characteristics are determined. Compared with the intact shell, changes in input and transmitted power flows with respect to the crack location and crack depth are obtained. At last the possible crack identification procedure is proposed.

2. Vibration of uncracked cylindrical shell

Consider an infinite uncracked thin-walled cylindrical shell, the coordinate system and the modal shapes are shown in Fig. 1. The free vibration motion of the thin shell can be described by the Flügge shell equations as [15]

$$u_{xx} + \frac{1+\mu}{2}u_{x\theta} + \frac{1-\mu}{2}v_{x\theta} + \mu w_x + K\left[\frac{1-\mu}{2}u_{\theta\theta} - w_{xxx} + \frac{1-\mu}{2}w_{x\theta\theta}\right] - \rho R^2(1-\mu^2)/Eu_{tt} = 0,$$

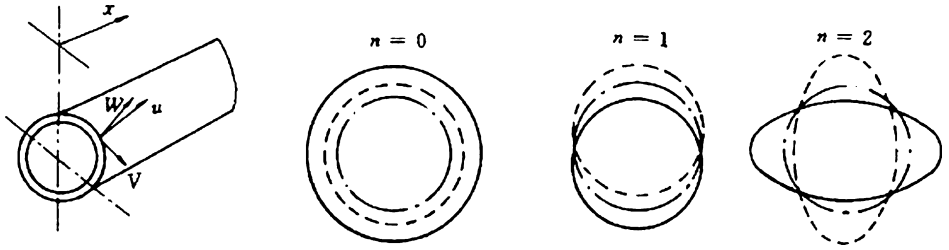

Fig. 1. Coordinate system and mode shapes of cylindrical shell.

$$\begin{aligned}
&\frac{1+\mu}{2}u_{x\theta}+v_{\theta\theta}+\frac{1-\mu}{2}v_{xx}+w_{\theta}+K\left[\frac{3(1-\mu)}{2}v_{xx}-\frac{3-\mu}{2}w_{xx\theta}\right]\\
&\quad-\rho R^2(1-\mu^2)/Ev_{tt}=0,\\
&K\left[\frac{1-\mu}{2}u_{x\theta\theta}-u_{xxx}-\frac{3-\mu}{2}v_{xx\theta}+w_{xxxx}+2w_{xx\theta\theta}+w_{\theta\theta\theta\theta}+2w_{\theta\theta}+w\right]\\
&\quad+\mu u_x+v_{\theta}+w+\rho R^2(1-\mu^2)/Ew_{tt}=0,
\end{aligned}\tag{1}$$

where u, v and w are shell displacements in the x, θ and r directions, respectively, R is the shell mean radius, h is the shell thickness, K is a thickness factor, $K=h^2/12R^2$, E is the Young's modulus, μ is the Poisson ratio, ρ is the density of the shell material, $(\,)_x=R(\partial(\,)/\partial x)$, $(\,)_\theta=\partial(\,)/\partial\theta$, $u_{tt}=\partial^2u/\partial t^2$.

Solutions of Eq. (1) can be expressed in the following forms as [16]

$$\left.\begin{aligned}
u&=\textstyle\sum_{n=0}^{\infty}u_n=\sum_{n=0}^{\infty}\sum_{s=1}^{m}U_{ns}\exp(-\mathrm{i}k_{ns}x+\mathrm{i}\omega t)\cos(n\theta)\\
v&=\textstyle\sum_{n=0}^{\infty}v_n=\sum_{n=0}^{\infty}\sum_{s=1}^{4}V_{ns}\exp(-\mathrm{i}k_{ns}x+\mathrm{i}\omega t)\sin(n\theta)\\
w&=\textstyle\sum_{n=0}^{\infty}w_n=\sum_{n=0}^{\infty}\sum_{s=1}^{m}W_{ns}\exp(-\mathrm{i}k_{ns}x+\mathrm{i}\omega t)\cos(n\theta)
\end{aligned}\right\},\tag{2}$$

where k_{ns} is the axial wavenumber and ω the driving frequency, n the circumferential modal number, s denotes a particular branch of the dispersion curves, $m=3$ for $n=0$ and $m=4$ for $n>0$. U_{ns}, V_{ns} and W_{ns} the wave amplitudes in the x, θ and r directions, respectively.

Substitution of Eq. (2) into the shell Eq. (1) results in the equations of motion of the shell in symmetric matrix form

$$[L_{3\times3}][U_{ns}\ V_{ns}\ W_{ns}]^{\mathrm{T}}=[0\ 0\ 0]^{\mathrm{T}},\tag{3}$$

where

$$[L_{3\times3}]=\begin{bmatrix}
-\lambda^2+a' & b'\lambda & c'\lambda^3+d'\lambda\\
b'\lambda & e'\lambda^2+f' & g'\lambda^2+h'\\
c'\lambda^3+d'\lambda & g'\lambda^2+h' & j'+k'\lambda^2+l'\lambda^4
\end{bmatrix},$$

$$\begin{aligned}
&a'=-(1-\mu)(1+K)n^2/2+\Omega^2,\ b'=(1+\mu)n/2,\ c'=-K,\\
&d'=\mu-K(1-\mu)n^2/2,\ e'=-(1-\mu)(1+3K)/2,\ f'=n^2-\Omega^2,\\
&g'=-(3-\mu)Kn/2,\ h'=n,\ j'=1+K(n^2-1)^2-\Omega^2,\\
&k'=-2n^2K,\ l'=K.
\end{aligned}$$

$\lambda=k_{ns}R$ is the non-dimensional axial wavenumber, $\Omega=\omega R/c_L$ is the non-dimensional driving frequency, and c_L is the extensional phase speed of the shell material.

Expansion of the determinant of the amplitude coefficient in Eq. (3) may provide the system characteristic equation, which is a bi-fourth polynomial equation about λ. From the polynomial equation, four pairs of wavenumbers can be obtained and can be written in the following form:

$$\lambda_i=\delta_i+ir_i,\ i=1,2,\ldots,8.\tag{4}$$

These wavenumbers can be separated into two groups. Each group consists of four waves. The first group describes backward waves associated with a semi-infinite shell ($-\infty < x < 0$), excited at the edge at $x = 0$, which includes the roots of $\delta_i < 0$, $r_i = 0$ and $r_i > 0$. The second group describes forward waves associated with a semi-infinite shell ($0 < x < \infty$) excited at the edge at $x = 0$, which includes the roots of $\delta_i > 0$, $r_i = 0$ and $r_i < 0$.

When λ_i is real or pure imaginary, one obtains a propagating wave or an evanescent near-field wave, respectively. If λ_i is complex in conjugate pairs, one obtains an attenuated standing wave, which means that the wave amplitudes decay in one direction but the waves propagate in both directions.

Substitution of the roots of the characteristic equation back into Eq. (3) and elimination of one variable by dividing the equation by W_{ns} can obtain the characteristic vectors

$$\Phi_{ns} = \frac{U_{ns}}{W_{ns}} = \frac{L_{13}L_{22} - L_{23}L_{12}}{L_{12}L_{21} - L_{11}L_{22}},$$
$$\Psi_{ns} = \frac{V_{ns}}{W_{ns}} = \frac{L_{23}L_{11} - L_{13}L_{12}}{L_{12}L_{21} - L_{11}L_{22}}.$$

The characteristic vectors denote the propagating nature of a particular wave.

Assume that the shell is excited by a harmonic line force F, acting at $x = 0$. The external force can be expressed as

$$F(\theta, t) = F_0 \cos(n\theta)\delta(0)\exp(\mathrm{i}\omega t). \tag{5}$$

Because of the symmetry of the shell and load, one can only consider the semi-infinite shell at the region $x \geqslant 0$. Four different waves will propagate along the positive direction, therefore for certain circumferential mode, four unknown coefficients W_{ns} exist in the system equation.

At any cross-section of the shell, there will exist four forces in the axial direction, which are axial force N_x, bending moment M_x, transverse shear force Q_x and torsional shear force $N_{x\theta}$. These forces for a particular circumferential mode n can easily be derived from the exact Flügge shell equations as [15]

$$\left.\begin{aligned}
N_x = N_{xn}\cos(n\theta) &= \frac{D}{R}\sum_{s=1}^{4}[\Phi_{ns}\lambda_s + \mu n\Psi_{ns} + \mu - K\lambda_s^2]W_{ns}\cos(n\theta)\\
M_x = M_{xn}\cos(n\theta) &= DK\sum_{s=1}^{4}[\lambda_s^2 - \mu n^2 - \Phi_{ns}\lambda_s - \mu n\Psi_{ns}]W_{ns}\cos(n\theta)\\
Q_x = Q_{xn}\cos(n\theta) &= \frac{D}{R}K\sum_{s=1}^{4}[(\lambda_s^3 - \mu n^2\lambda_s - \Phi_{ns}\lambda_s^2 - \mu n\Psi_{ns}\lambda_s)\\
&\quad -(1-\mu)(2n^2\lambda_s + 0.5n^2\Phi_{ns} + 1.5n\Psi_{ns}\lambda_s)]W_{ns}\cos(n\theta)\\
N_{x\theta} = N_{x\theta n}\sin(n\theta) &= \frac{D(1-\mu)}{R\quad 2}\sum_{s=1}^{4}[-n\Phi_{ns} + (1+3K)\Psi_{ns}\lambda_s + 3kn\lambda_s]W_{ns}\sin(n\theta)
\end{aligned}\right\} \tag{6}$$

where D is tensional rigid, $D = Eh/(1-\mu^2)$.

According to the symmetry, four boundary conditions at cross-section $x = 0$ can be given as

$$\left.\begin{aligned} u &= 0\\ \partial w/\partial x &= 0\\ N_{x\theta} &= 0\\ Q_x &= -F/2 \end{aligned}\right\}. \tag{7}$$

Therefore, the four coefficients can be derived and the vibration of the uncracked cylindrical shell can be determined.

3. Vibration of cracked cylindrical shell

3.1. Crack model of cylindrical shell

Assume there exists a circumferential surface crack with uniform depth of a in an infinite cylindrical shell, the crack running through the θ direction. To avoid nonlinear, it is assumed that the surface crack is always open. The distance between the cross-section of crack and the cross-section of the line force is c. One can isolate a longitudinal element of unit width from the shell, as shown in Fig. 2.

The surface crack in the shell can be modeled as a distributed line spring [17]. The presence of the crack in the shell will cause the local flexibility. The flexibility of the spring is a function of the local dimensions and the elastic properties of the cracked region. The local flexibility in the shell will result in the discontinuity of the generalized displacement at the both sides of crack's section, then the local deformation at the cracked region can be identified according to the local compliance [3]

$$\delta_i^R - \delta_i^L = C_{ij} P_i, \tag{8}$$

where $\delta_i{}^L$ and $\delta_i{}^R$ are the generalized displacement to the left and to the right of the cracked section of the shell, respectively. C_{ij} and P_i denote the local compliance and the generalized force, respectively.

The Paris equation gives the generalized displacement U_i as a function of the strain energy release rate J

$$U_i = \frac{\partial}{\partial P_i} \int_0^a J \, \mathrm{d}a. \tag{9}$$

Therefore, the compliance can be expressed as

$$C_{ij} = \frac{\partial U_i}{\partial P_j} = \frac{\partial^2}{\partial P_i \partial P_j} \int_0^a J \, \mathrm{d}a. \tag{10}$$

In addition, expressions for the strain energy release ratio can be directly expressed as function of the stress intensity factor [18]

$$J = \frac{1}{E'} \left[\left(\sum_{n=1}^{4} K_{\mathrm{I}n} \right)^2 + \left(\sum_{n=1}^{4} K_{\mathrm{II}n} \right)^2 + k \left(\sum_{n=1}^{4} K_{\mathrm{III}n} \right)^2 \right], \tag{11}$$

where $K_{\mathrm{I}n}$, $K_{\mathrm{II}n}$, $K_{\mathrm{III}n}$ are the stress intensity factor for modes of I, II and III, respectively, $E' = E$ for plane stress, $E' = E/(1-\mu^2)$ for plane strain, $k = 1+\mu$.

The stress intensity factors of different modes can be tabulated as shown in Table 1 [18].

By substituting the stress intensity factors tabulated in Table 1 into Eq. (11) and differentiating twice with respect to P_i and P_j, one can obtain the local compliance pertinent to different internal force.

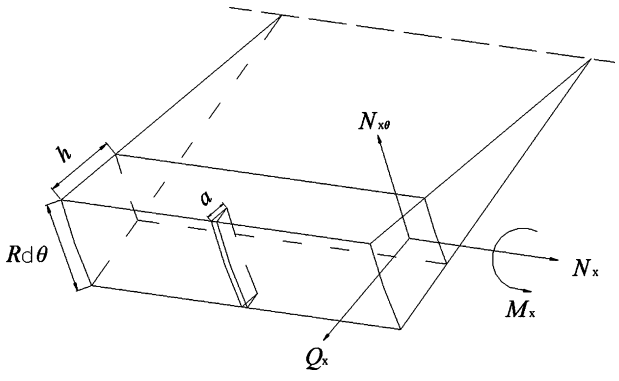

Fig. 2. Geometry of an element of cracked shell.

Table 1
Stress intensity factor [17]

	N_x	M_x	Q_x	$N_{x\theta}$
$K_{\mathrm{I}n}$	$F_1 N_x\sqrt{\pi a}/h$	$6F_2 M_x\sqrt{\pi a}/h^2$	0	0
$K_{\mathrm{II}n}$	0	0	$1.5F_3 Q_x(1-0.5\bar{a}^2)\sqrt{\pi a}/h$	0
$K_{\mathrm{III}n}$	0	0	0	$F_4 N_{x\theta}\sqrt{\pi a}/h$

where F_n are the correction functions, which are dimensionless function of the crack depth ratio, and are given by [17].

$$
\begin{aligned}
&F_1 = F_4[0.752 + 1.287\alpha + 0.37(1-\sin\alpha)^3]/\cos\alpha,\\
&F_2 = F_4[0.923 + 0.199(1-\sin\alpha)^4]/\cos\alpha,\\
&F_3 = (1.122 - 0.561\bar{a} + 0.085\bar{a}^2 + 0.18\bar{a}^3)/\sqrt{1-\bar{a}},\\
&F_4 = \sqrt{\tan\alpha/\alpha},\\
&\bar{a} = a/h,\ \alpha = \pi\bar{a}/2.
\end{aligned}
$$

When $P_j = P_i = N_x$, the tensile component of the compliance matrix with respect to N_x can be obtained as

$$C_{11} = 2\pi/E' \int_0^a F_1^2 a/h^2\,\mathrm{d}a. \tag{12}$$

Similarly, the compliance with respect to M_x is

$$C_{22} = 72\pi/E' \int_0^a F_2^2 a/h^4\,\mathrm{d}a. \tag{13}$$

For Q_x and $N_{x\theta}$, one can get

$$C_{33} = 4.5\pi/E' \int_0^a F_3^2(1-0.5\bar{a}^2)^2 a/h^2\,\mathrm{d}a, \tag{14}$$

$$C_{44} = 2\pi k/E' \int_0^a F_4^2 a/h^2\,\mathrm{d}a. \tag{15}$$

Considering the coupling of longitudinal, bending and transverse shear displacement, for $P_j \neq P_i$, we have

$$
\begin{aligned}
&C_{12} = 12\pi/E' \int_0^a F_1 F_2 a/h^3\,\mathrm{d}a,\\
&C_{21} = C_{12},\ C_{13} = C_{14} = C_{24} = C_{34} = 0,\\
&C_{31} = C_{13},\ C_{41} = C_{14},\ C_{42} = C_{24},\ C_{43} = C_{34}.
\end{aligned} \tag{16}
$$

Thus, the local compliance matrix can be obtained, which is a 4×4-dimensional matrix. In Fig. 3, the diagonal elements C_{ii} of the local compliance matrix with different crack depth are plotted together. It can be seen from the figure that the local compliances increase with increasing crack relative depth a/h. In addition, the compliance C_{22} with respect to bending moment is much larger than any others. It denotes that the local compliance with respect to bending moment in the shell is dominant in the local compliance matrix, which is consistent with the results obtained by Gounaris and Dimarogonas [3] in the cracked beam structures.

3.2. Wave motion in the cracked cylindrical shell

When the harmonic line force F is acted on the shell at cross-section of $x = 0$ and the crack is located at cross-section of $x = c$, the infinite shell can be divided into three regions a–c: the semi-infinite region of $x \leqslant 0$, finite region of $0 \leqslant x \leqslant c$ and the semi-infinite region of $x \geqslant c$. From the origin, four waves will propagate along the negative direction and other four waves along the positive direction. When the forward waves incident on the discontinuity of the crack, there will exist four transmitted waves and four reflected waves. Theoretically,

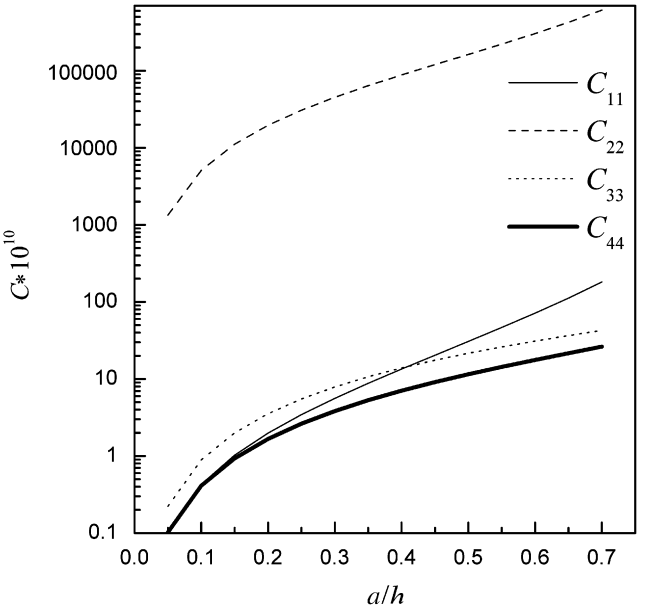

Fig. 3. Local flexibility versus crack's depth.

the incident waves of mode order n will generate only waves with an identical mode order when they meet the discontinuity of the crack. However, the boundary conditions at the cross-section of discontinuity will be satisfied by the inclusion of near fields due to waves below cut-on as well as propagating waves [16]. Consequently, when the forward waves incident on the discontinuity of the crack, there will exist four transmitted waves and four reflected waves with the same mode order. Thus, under the excitation of the harmonic line force, there are four waves of unknown coefficients in the region of $x \leqslant 0$, eight unknown waves in the region of $0 \leqslant x \leqslant c$ and four unknown waves in the region of $x \geqslant c$.

In the semi-infinite region of $x \leqslant 0$, for specified circumferential modal number n, the axial displacement u_a can be expressed as

$$u_a = \sum_{s=1}^{4} \Phi_{ns} W_{ns} \exp(\mathrm{i}k_{ns}x + \mathrm{i}\omega t) \cos(n\theta), \tag{17}$$

where the subscript a denotes the regions $a(x \leqslant 0)$, the characteristic vectors Φ_{ns} and axial wavenumber k_{ns} can be obtained from Section 2, only the four coefficients W_{ni} $(i = 1,2,3,4)$ are unknown.

In the finite region of $0 < x < c$, the response may be expressed in the superposition of eight possible wave, therefore the axial displacement u_b can be expressed as

$$\begin{aligned} u_b = & \sum_{s=1}^{4} \Phi_{ns} W_{n(s+4)} \exp(-\mathrm{i}k_{ns}x + \mathrm{i}\omega t) \cos(n\theta) \\ & + \sum_{s=5}^{8} \Phi_{n(s-4)} W_{n(s+4)} \exp[\mathrm{i}k_{n(s-4)}(x-c) + \mathrm{i}\omega t] \cos(n\theta), \end{aligned} \tag{18}$$

where the subscript b denotes the finite regions $b(0 < x < c)$ and eight coefficients W_{ni} $(i = 5,6,7,\ldots,12)$ are unknown.

For the semi-infinite region $c(x \geqslant c)$, four waves with unknown amplitudes will propagate along the positive direction. The axial displacement is

$$u_c = \sum_{s=1}^{4} \Phi_{ns} W_{n(s+12)} \exp[-\mathrm{i}k_{ns}(x-c) + \mathrm{i}\omega t] \cos(n\theta), \tag{19}$$

where exist four unknown coefficients W_{ni} $(i = 13,14,15,16)$.

Similar expressions can be written for the radial and circumferential components of displacement in region a, b and c. The expressions of the radial and circumferential displacements also contain the sixteen unknown coefficients W_{ni} ($i = 1,2,3,\ldots,16$). Consequently, the internal forces, axial force N_x, bending moment M_x, transverse shear force Q_x and torsional shear force $N_{x\theta}$ in any cross-section of the cracked shell can be expressed by using the sixteen unknown coefficients.

In order to solve these 16 unknown wave coefficients, 16 boundary conditions are required.

At the cross-section of $x = 0$, the continuous conditions of internal forces are

$$N_x^R = N_x^L,\ M_x^R = M_x^L,\ N_{x\theta}^R = N_{x\theta}^L,\ Q_x^R = Q_x^L + F, \tag{20}$$

where superscripts R and L represent the right side and left side of the cross-section, respectively.

The axial, tangential, radial and angular displacements are continuous, respectively, at the cross-section of $x = 0$, so

$$u^R = u^L,\ v^R = v^L,\ w^R = w^L,\ \partial w^R/\partial x = \partial w^L/\partial x. \tag{21}$$

The detail expression of the radial displacement's continuous condition, for example, can be written as

$$\sum_{s=1}^{4} \Phi_{ns} W_{n(s+4)} \exp(-\mathrm{i}k_{ns}x + \mathrm{i}\omega t) + \sum_{s=5}^{8} \Phi_{n(s-4)} W_{n(s+4)} \exp[\mathrm{i}k_{n(s-4)}(x-c) + \mathrm{i}\omega t]\Big|_{x=0} = \sum_{s=1}^{4} W_{ns} \exp(\mathrm{i}k_{ns}x + \mathrm{i}\omega t)\cos(n\theta)\Big|_{x=0}. \tag{22}$$

At the cross-section $x = c$ of the crack, the continuity of axial force, angular bending moment, transverse shear, and torsional shear should be satisfied, so

$$N_x^R = N_x^L,\ M_x^R = M_x^L,\ Q_x^R = Q_x^L,\ N_{x\theta}^R = N_{x\theta}^L. \tag{23}$$

The crack induces the discontinuity of the displacement at $x = c$, and the local compliance matrix is deduced above. So the discontinuity at the both sides of the crack can be written as

$$\begin{bmatrix} u^R - u^L \\ \partial w^R/\partial x - \partial w^L/\partial x \\ w^R - w^L \\ v^R - v^L \end{bmatrix} = [C_{4\times4}] \begin{bmatrix} N_x \\ M_x \\ Q_x \\ N_{x\theta} \end{bmatrix}. \tag{24}$$

From the above analysis, it is clear that at the cross-sections of $x = 0$ and c there are eight boundary conditions, respectively. Therefore, by substituting the expressions of displacements and internal forces into the sixteen equations, the unknown wave coefficients W_{ni} ($i = 1,2,3,\ldots,16$) will be solved. Consequently, the wave motion in the cracked shell structure can be determined. It should be noted that the real wavenumber wave as well as complex wavenumber wave are included when solving the system equations using the boundary conditions at $x = 0$ and c. For the case of circumferential mode $n = 0$, the motion in the u, w direction is uncoupled with the motion in the v direction, there exit twelve possible waves in axial direction and six boundary conditions can be obtained at the cross-sections of $x = 0$ and c, respectively.

4. Vibrational power flow in cylindrical shell

When the shell structure is excited by harmonic external force, the vibrational power flow input by the external force propagates along the wall of the shell continuously. When the external force F and the velocity V are harmonic at a point, the time averaged power flow is [12]

$$P_{in} = \frac{1}{2}\mathrm{Re}\{FV^*\}, \tag{25}$$

where Re(*) expresses the real part of a complex value, an asterisk denotes the complex conjugate.

For the uncracked or cracked cylindrical shell, when a harmonic external force $F(\theta,t)=F_0\cos(n\theta)\,\delta(0)\exp(\mathrm{i}\omega t)$ is applied to the shell wall along radial direction, the radial displacement of the shell wall at $x=0$ can be obtained from above analysis. Then the input power flow from this driving force can be written as

$$P_{in}=\frac{1}{2}\int_0^{2\pi}\mathrm{Re}\{\mathrm{i}\omega F_0\cos(n\theta)W^*(0)(\cos n\theta)\}R\mathrm{d}\theta=\frac{\pi R}{2\varepsilon_n}\mathrm{Re}\{\mathrm{i}\omega F_0 W^*(0)\},\tag{26}$$

where $\varepsilon_n=1/2$ for $n=0$ and $\varepsilon_n=1$ for $n>0$.

The non-dimensional power flow is defined as

$$P'_{in}=\frac{P_{in}}{F_0^2\pi}\sqrt{\rho ER^2(1-\mu^2)}.\tag{27}$$

Fuller [19] has demonstrated that the input power flow of an infinite cylindrical shell excited by a radial line force can be calculated by using the method of residues, while for the cracked infinite shell, the input power flow cannot be formulated by using the method of residues. In this research the input power flows of both uncracked shell and cracked shell are determined from the motion equation and the boundary conditions as shown in above sections.

Along with the power input into the shell, power flow will also be transmitted along the shell axial direction. The uncracked and cracked shell's displacements in the x, θ and r directions have bend derived in Sections 2 and 3, respectively, therefore the four internal forces, axial force N_x, bending moment M_x, transverse shear force Q_x and torsional shear force $N_{x\theta}$ in any cross-section of the uncracked and cracked shell can be obtained. Meanwhile, corresponding to the four internal forces, the generalized velocities, $\mathrm{i}\omega u$, $\mathrm{i}\omega\partial\omega/\partial x$, $\mathrm{i}\omega w$ and $\mathrm{i}\omega v$ can be obtained, respectively. As a results, at any cross-section the vibrational power flow transmitted by these forces are respectively expressed as

$$\begin{aligned}
P_{N_x}&=\frac{1}{2}\int_0^{2\pi}\mathrm{Re}\{\mathrm{i}\omega N_{xn}\cos(n\theta)U^*_{xn}(\cos n\theta)\}R\,\mathrm{d}\theta=\frac{\pi R}{2\varepsilon_n}\mathrm{Re}\{\mathrm{i}\omega N_{xn}U^*_{xn}\},\\
P_{M_x}&=\frac{1}{2}\int_0^{2\pi}\mathrm{Re}\{\mathrm{i}\omega M_{xn}\cos(n\theta)(\partial W^*_{xn}(x)/\partial x)(\cos n\theta)\}R\,\mathrm{d}\theta=\frac{\pi R}{2\varepsilon_n}\mathrm{Re}\{\mathrm{i}\omega M_{xn}(\partial W^*_{xn}(x)/\partial x)\}\\
P_{Q_x}&=\frac{1}{2}\int_0^{2\pi}\mathrm{Re}\{\mathrm{i}\omega Q_{xn}\cos(n\theta)W^*_{xn}(x)(\cos n\theta)\}R\,\mathrm{d}\theta=\frac{\pi R}{2\varepsilon_n}\mathrm{Re}\{\mathrm{i}\omega Q_{xn}W^*_{xn}\},\\
P_{N_{x\theta}}&=\frac{1}{2}\int_0^{2\pi}\mathrm{Re}\{\mathrm{i}\omega N_{x\theta n}\cos(n\theta)V^*_{xn}(x)(\cos n\theta)\}R\,\mathrm{d}\theta=\frac{\pi R}{2\varepsilon_n}\mathrm{Re}\{\mathrm{i}\omega N_{x\theta n}V^*_{xn}\}.
\end{aligned}$$

The total transmitted power flow in the shell is

$$P_{\mathrm{tr}}=P_{N_x}+P_{M_x}+P_{Q_x}+P_{N_{x\theta}}.\tag{28}$$

Therefore, the input power flow and transmitted power flow in the uncracked and cracked shell can be derived from above analysis. The change of the power flow in the cracked cylindrical shell may be related to the position and the depth of the crack. The relationship between the crack parameters and the power flow characteristics can be revealed via the research on the power flow characteristics of different crack parameters.

5. Numerical results and discussions

In this research, an undamped infinite thin-walled cylindrical shell is considered. The parameters of the shell are shown as follows, modulus of elasticity $E=1.92\times10^{11}$ Pa, Poisson's ratio $\mu=0.3$, mass density $\rho=7800\,\mathrm{kg/m^3}$, a thickness to radius ratio of $h/R=0.05$. The unit harmonic line force F is located at $x=0$. A circumferential surface crack with uniform depth of a is located at $x=c$.

5.1. Input power flow of uncracked and cracked shell

The dispersion characteristics including the complex wavenumbers of the cylindrical shell were discussed in detail by Fuller [16], and the power flow characteristics in the intact shell together with the measurement of power flow in the shell have been discussed by many researchers [20–24]. The uncracked shell's input power flow is calculated to compare with that of the cracked shell in this paper.

Fig. 4 shows the non-dimensional input power flow of uncracked and cracked shell under different circumferential modal number ($n = 0$,1,2 and 5 in Figs. 4(a)–(d), respectively), in which the solid line represents the non-dimensional input power flow of uncracked shell and the dashed line represents the cracked shell's non-dimensional input power flow with the crack parameters of $a/h = 0.5$ and $c/R = 1$. For the uncracked cylindrical shell, there exists cut off frequency, below which there is no energy input into the shell structure, and the cut off frequency increases with increasing circumferential modal number. For example, for the circumferential mode of $n = 0$ there is no cut off frequency, while for $n = 2$ and 5 circumferential modes the non-dimensional cut off frequencies are near 0.05 and 0.3, respectively. For the $n = 0$ circumferential mode, the non-dimensional input power flow curve has one peak near the ring frequency ($\Omega = 1$) of the shell. However, for any circumferential mode of $n > 0$, the non-dimensional input power flow curve has two peaks over the frequency range. When the circumferential mode is small ($n = 1$,2), the first peak is near the ring frequency ($\Omega = 1$) of the shell, as can be seen from Figs. 4(b) and (c). For the high circumferential modes, for example, $n = 5$, however, the first peak is not near the ring frequency but near the cut off frequency. For the $n > 0$ circumferential modes, the second peak is associated with the cutting on of the longitudinal type shell wave [19]. For example, for the circumferential modes $n = 2$, the second peak is near $\Omega = 2.2$, which is corresponding to the cutting on frequency of the second propagating wave.

For the cracked shell, there still exist cut off frequencies for different circumferential modes, and the cut-off frequency of cracked shell is identical with that of uncracked shell for the same circumferential mode. In addition, the non-dimensional input power flow curve of cracked shell also have obvious peaks at corresponding frequencies, as can be seen from Fig. 4. But the presence of the crack changes the input power flow characteristics observably. It can be found that for different circumferential modes, the non-dimensional input power flow of cracked shell fluctuates around that of uncracked shell with the increase of the driving frequency, though the fluctuation is not very evident at low frequencies. For the low order circumferential modes ($n = 0$,1 and 2), the peak value near the ring frequency of cracked shell is bigger than that of uncracked shell, and for the $n > 0$ circumferential modes, the value of the second peak of cracked shell is also bigger than that of uncracked shell. This is because the presence of the crack induces the decrease of the rigidity of the shell.

In the following cases, the circumferential modal number $n = 1$ will be always chosen. In order to investigate the influence of crack's position on the input power flow of the shell, the crack's relative depth is kept constant at $a/h = 0.3$ and the crack's position is changed, as shown in Fig. 5. From the figure it is clear that when the relative position c/R increases from 1 to 2, the non-dimensional input power flow curve fluctuates more and more quickly over the same frequency range. In Fig. 6 the crack's relative position is kept constant at $c/R = 1$ and the crack's relative depth a/h is changed from 0.1 to 0.5 to investigate the influence of crack's depth on the input power flow. The figure shows that the degree of fluctuation increases when the crack relative depth increases. This is because the increase of the local flexibility induces the increase of response of the shell.

In order to obtain the crack's information (position and depth) from the changes of power flow characteristics in the shell, one can define the ratio of cracked shell's input power flow to uncracked shell's input power flow as the normalized input power flow R_c. The normalized input power flows versus crack location and depth are shown in three-dimensional plot of Figs. 7 and 8. Because the shell is infinite in length, the crack's relative position c/R is just chosen from 0 to 0.5 to demonstrate the relationship between the crack's information and the normalized input power flow. The non-dimensional driving frequency in Figs. 7 and 8 is 0.7 and 2, respectively. From the two figures, it is clear that the crack location and crack depth are both highly related to the normalized input power flow R_c, and the fluctuation of the plots becomes obvious with increasing of the crack depth. From the comparison between Figs. 7 and 8, it can be found that the number of the surface's peaks increases with increasing the driving frequency at the same range of c/R, which denotes the normalized input power flow are more sensitive to the crack position at higher frequencies.

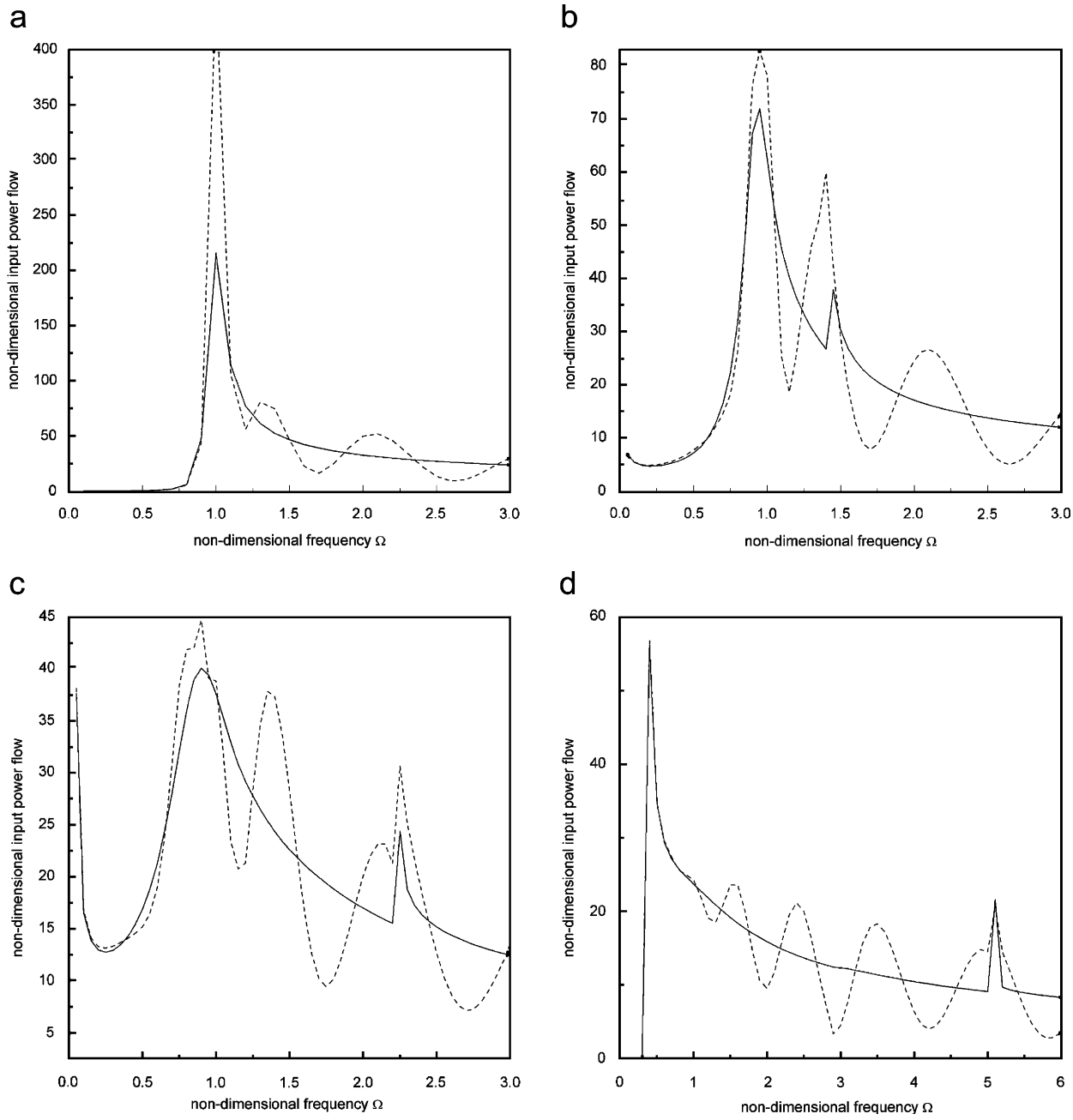

Fig. 4. Non-dimensional input power flow of uncracked shell (solid line) and cracked shell (dotted line) crack parameteristics: $a/h = 0.5$, $c/R = 1$.

5.2. Transmission of power flow in cracked shell

When the force is acting on the shell structure, the energy will propagate along the wall of the shell continuously. At any cross-section of the shell, the vibrational power flow is transmitted by four internal forces. For the intact infinite shell, the input power flow is divided two equal parts propagating along positive and negative directions, respectively. Because the damping is not considered in this paper, the total transmitted power flow is always the half of the input power flow and independent of the distance. For the

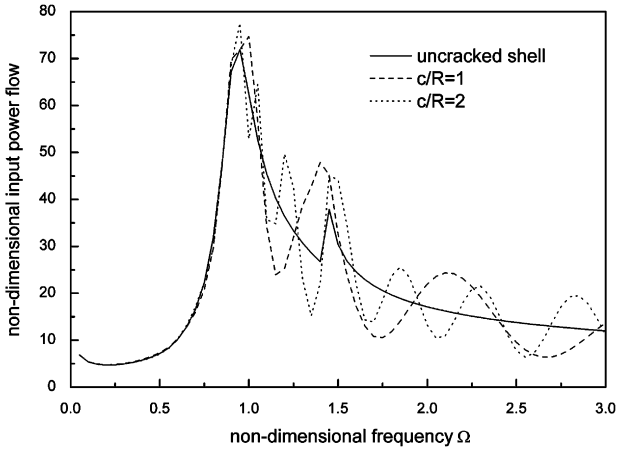

Fig. 5. Non-dimensional input power flow of uncracked shell and cracked shell ($n = 1$, $a/h = 0.3$).

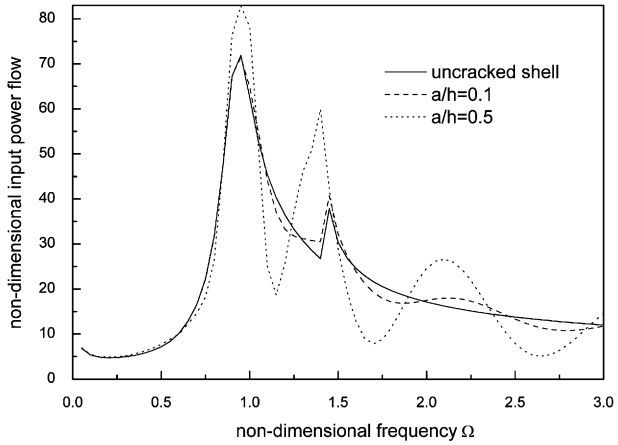

Fig. 6. Non-dimensional input power flow of uncracked shell and cracked shell ($n = 1$, $c/R = 1$).

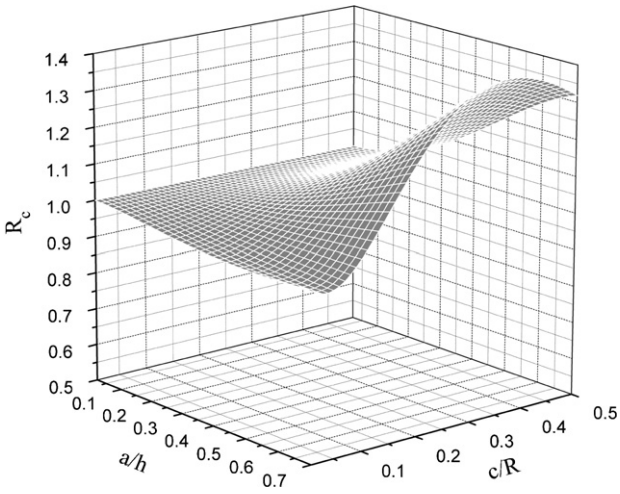

Fig. 7. Normalized input power flow of cracked shell ($n = 1$, $\Omega = 0.7$).

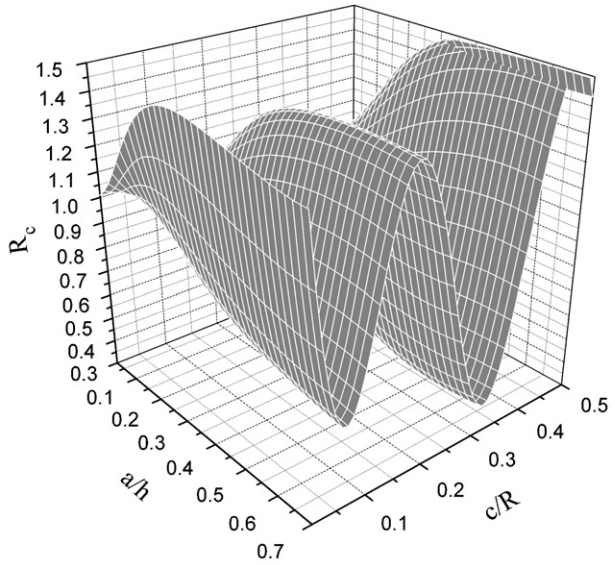

Fig. 8. Normalized input power flow of cracked shell ($n = 1$, $\Omega = 2$).

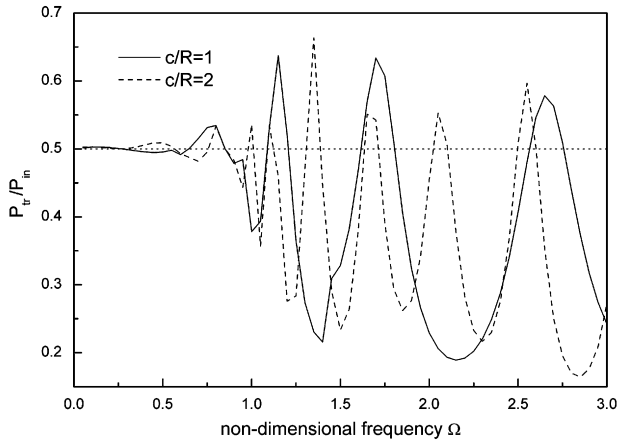

Fig. 9. Ratio of input power flow to transmitted power flow of cracked shell ($n = 1$, $a/h = 0.3$).

cracked shell, the transmitted power flows along both sides of the origin are not equal due to the presence of the crack, though the sum of the transmitted power flows along two directions is equal to the input power flow. The calculation results also show that the total transmitted power flow of cracked shell along one direction is independent of distance due to the undamped shell.

Figs. 9 and 10 show the ratio of transmitted power flow along positive direction to input power flow P_{tr}/P_{in} with different crack parameters. The dotted straight lines ($P_{tr}/P_{in} = 1/2$) in the two figures represent the uncracked shell's transmitted power flow ratio. The relative crack depth is kept constant at $a/h = 0.3$ in Fig. 9 while the relative crack position is kept constant at $c/R = 1$ in Fig. 10. It can be seen that the transmitted power flow ratio curves of cracked shell fluctuate around the straight line $P_{tr}/P_{in} = 1/2$ in the two figures, and the fluctuation becomes apparent at higher frequencies. It also can be seen that the characteristics of the transmitted power flow ratio curves are similar to those of the input power flow curves when increasing c/R and a/h, respectively.

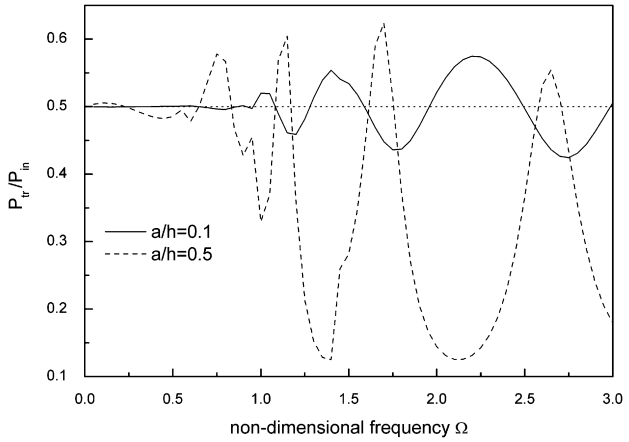

Fig. 10. Ratio of input power flow to transmitted power flow of cracked shell ($n = 1$, $c/R = 1$).

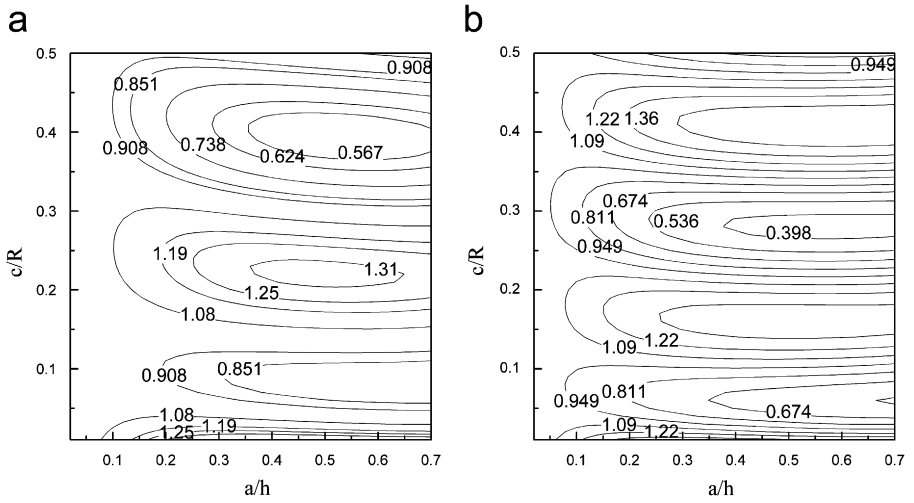

Fig. 11. Contours of normalized input power flow at different non-dimensional driving frequencies: (a) $\Omega = 1.2$; (b) $\Omega = 2.5$.

5.3. Crack detection procedure using power flow

Based on above analysis, it can be found that the existence of the crack causes the change of power flow characteristics in the shell. Both the crack location and depth have influences on the input and transmitted power flow. It denotes that certain input power flow or transmitted power flow could correspond to different combination of crack's location and depth. The contour lines of the normalized input power flow could be plotted in one figure from different combinations of crack location and depth at some specified frequencies via the analytical solutions above, the figure having the crack location and depth as its axes. Figs. 11(a) and (b) show the contour lines of normalized input power flow of cracked shell with non-dimensional driving frequency of 1.2 and 2.5, respectively. In order to be clear and readable, only parts of the contour lines are plotted and labeled. It can be found that the location and depth corresponding to any point on the curves would become the possible crack location and depth. A crack should and must belong to one contour line for each driving frequency.

For some existent crack in the shell structure, the crack depth and location are both unknown. But the input power flow of the cracked shell at specified driving frequencies may be measured first, and then the normalized input power flow at two different driving frequencies can be obtained directly as the input. Therefore, contour

lines corresponding to the obtained normalized input power flow at two driving frequencies can be plotted together, and the intersection point would indicate the location and depth of the crack. When more than one intersection point is obtained from the merged figure, the contour line from another driving frequency could be added into the figure and the intersection point of the three contour lines could be used to uniquely obtain the final point, which would indicate the crack location and depth. Usually, contour lines from three different frequencies will be sufficient to identify the crack.

In order to explain the crack detection procedure clearly, two examples are presented in this paper. In the first case, it is assumed that a cylindrical shell with relative crack depth $a/h = 0.4$ and relative crack position $c/R = 0.15$ is considered. In this case, from the numerical results in Section 5.1 the normalized input power flow for the $\Omega = 0.7$ non-dimensional frequency is 1.04 and is 0.71 for the $\Omega = 1.2$ non-dimensional frequency. According to these results, the solid contour line with the value of 1.04 from the $\Omega = 0.7$ driving frequency can be plotted in Fig. 12. The dashed contour line with the value of 0.71 from the non-dimensional driving frequency of 1.2 is also plotted in the same figure. It can be found from the figure that there is only one intersection point, the abscissa and the ordinate of which respectively represent that the relative crack depth is 0.4 and the relative crack position is 0.15. Therefore normalized input power flows from only two driving frequencies are sufficient for crack detection in this case.

In the second case, it is assumed that when non-dimensional frequency is 0.7, the normalized input power flow is 1.04 while the normalized input power flow is 1.16 with the non-dimensional driving frequency of 1.2 for certain unknown crack. Accordingly, the solid contour line with the value of 1.04 at the non-dimensional driving frequency of 1.04 can be plotted in Fig. 13, the dashed contour line with the value of 1.16 at driving frequency of 1.2 being plotted in the same figure. From this figure, it can be seen that there are two intersection points for these two contours, which are labeled 'A' and 'B', respectively. In order to uniquely decide the final point, the contour line at another frequency will be used. Considering the normalized input power flow of the cracked shell is 0.89 at the non-dimensional driving frequency of 1.5, the dotted contour with the value of 0.89 at 1.5 non-dimensional driving frequency can be used to uniquely obtain the final point, as can be seen from Fig. 14. The three contour lines intersect at point 'A', which indicates that the relative depth a/h is 0.2 and the relative crack position c/R is 0.35 in this case. So the crack's depth and location may be identified according to the input power flow contour diagrams. In this research the shell is infinite; therefore, the relative distance is chosen only from 0 to 0.5 to give a demonstration of identification procedure. For the finite shell, the crack position in the contour diagram will be constructed from one end to the other end to detect the crack. Besides the input power flow, the contour lines of transmitted power flow may be also constructed to identify the crack in the shell.

From the above examples, it can be found that the power flow characteristics are not very sensitive to very small cracks ($a/h < 0.1$). Therefore, the application of the method may be suit for the cases of relative crack

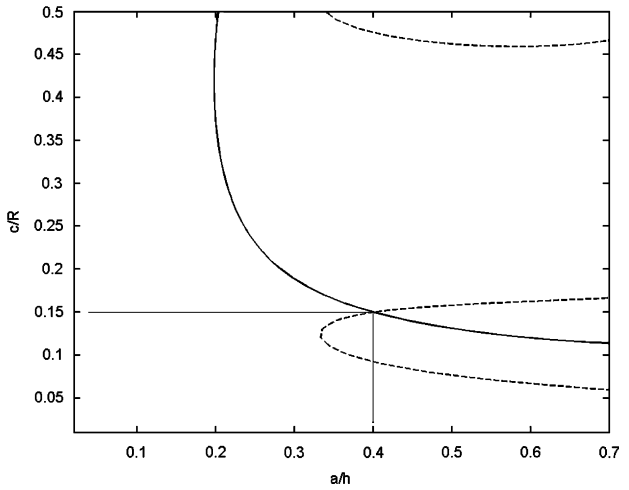

Fig. 12. Crack identification by contours of normalized input power flow from two different non-dimensional driving frequencies: $\Omega = 0.7$, $R_c = 1.04$ (solid line); $\Omega = 1.2$, $R_c = 0.71$ (dashed line), the intersection point denotes that $c/R = 0.15$, $a/h = 0.4$.

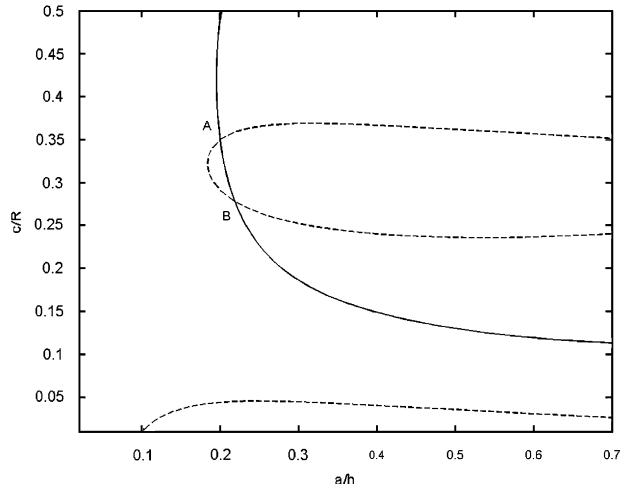

Fig. 13. Contours of normalized input power flow from two different non-dimensional driving frequencies: $\Omega = 0.7$, $R_c = 1.04$ (solid line); $\Omega = 1.2$, $R_c = 1.16$ (dashed line).

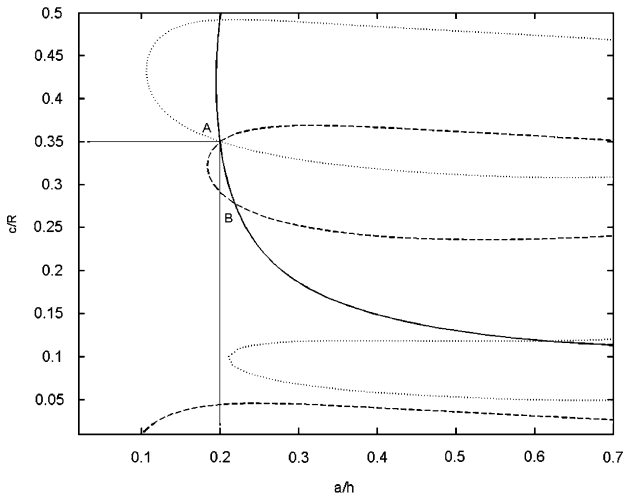

Fig. 14. Crack identification by contours of normalized input power flow from three different non-dimensional driving frequencies: $\Omega = 0.7$, $R_c = 1.04$ (solid line); $\Omega = 1.2$, $R_c = 1.16$ (dashed line) $\Omega = 1.5$, $R_c = 0.89$ (dotted line), point 'A' denotes that $c/R = 0.35$, $a/h = 0.2$.

depth $a/h \geqslant 0.1$. However, like most vibration-based damage detection methods, the method proposed in this paper, as a global crack detection method, provides a simple and useful tool to detect a crack without the access of the whole structure. In addition, just the input powers in the structures are required to be measured, therefore one impendence head placed on a structure could give the values of input power flows at different frequencies, unlike the methods based on the mode shape (curvature mode shape, strain mode shape, etc.), which always need to measure responses at a large number of locations and pose practical difficulties due to limitations in the numbers of sensors and the capability of accurate measurement.

6. Conclusions

This paper has presented an approach to analyze the wave and vibrational power flow characteristics in cracked cylindrical shell structures. The case of an infinite thin cylindrical shell with a circumferential surface crack was considered. By modeling the crack with line spring, the local compliance matrix due to the presence

of the crack was deduced from fracture mechanics. Changes in input and transmitted power flows with respect to the crack location and crack depth were obtained. The results revealed that the vibrational power flow of cracked cylindrical shell is quite related to the crack's characteristic parameters. Contour plots of normalized input power flow were used to identify the crack. The numerical result showed that the proposed method could successfully identify the crack location and depth.

It should be pointed out that in this study the external force is assumed to be a harmonic line-distributed force for convenience, actually the external force of other types can also be acted on the shell, for example, the radial point force, which can be obtained from the transformation of the harmonic line-distributed force and the measurement of the input and transmitted power flow excited by which has been researched by Ming [23]. Therefore, this new method can be applied in principle to the case of other force excitations. The research in this paper provides an alternative method to identify the crack in cylindrical shell structures by measuring the vibrational power flow. Further work will be done to investigate the cracked finite cylindrical shell's input and transmitted power flow characteristics and some experiments will be implemented to verify the feasibility of the approach.

Acknowledgments

The authors are pleased to acknowledge the support of the National Natural Science Foundation of PR China (Contract No. 50375059).

References

[1] S.W. Doebling, C.R. Farrar, M.B. Prime, Summary review of vibration-based damage identification methods, *Shock and Vibration Digest* 30 (2) (1998) 91–105.
[2] A.D. Dimarogonas, Vibration of cracked structures: a state of the art review, *Engineering Fracture Mechanics* 55 (5) (1996) 831–857.
[3] G. Gounaris, A. Dimarogonas, Finite element of a cracked prismatic beam for structural analysis, *Computers & Structures* 28 (3) (1988) 309–313.
[4] T.D. Chaudhari, S.K. Maiti, Study of vibration of geometrically segmented beams with and without crack, *International Journal of Solids and Structures* 37 (5) (2000) 761–779.
[5] S.E. Khadem, M. Rezaee, An analytical approach for obtaining the location and depth of an all-over part-through crack on externally in-plane loaded rectangular plate using vibration analysis, *Journal of Sound and Vibration* 230 (2) (2000) 291–308.
[6] E. Douka, S. Loutridis, A. Trochidis, Crack identification in plates using wavelet analysis, *Journal of Sound and Vibration* 270 (1–2) (2004) 279–295.
[7] M. Krawczuk, M. Palacz, W. Ostachowicz, Wave propagation in plate structures for crack detection, *Finite Elements in Analysis and Design* 40 (9–10) (2004) 991–1004.
[8] M.G. Srinivasan, C.A. Kot, Damage index algorithm for a circular cylindrical shell, *Journal of Sound and Vibration* 215 (3) (1998) 587–591.
[9] K. Nikpour, Diagnosis of axisymmetric cracks in orthotropic cylindrical shells by vibration measurement, *Composites Science and Technology* 39 (1) (1990) 45–61.
[10] T. Marwala, Damage identification using committee of neural networks, *Journal of Engineering Mechanics* 126 (1) (2000) 43–50.
[11] A. Roytman, O. Titova, An analytical approach to determining the dynamic characteristics of a cylindrical shell with closing cracks, *Journal of Sound and Vibration* 254 (2) (2002) 379–386.
[12] T.Y. Li, W.H. Zhang, T.G. Liu, Vibrational power flow analysis of damaged beam structures, *Journal of Sound and Vibration* 242 (1) (2001) 59–68.
[13] T.Y. Li, T. Zhang, J.X. Liu, et al., Vibrational wave analysis of infinite damaged beams using structure-borne power flow, *Applied Acoustics* 65 (1) (2004) 91–100.
[14] T.Y. Li, J.X. Liu, T. Zhang, Vibrational power flow characteristics of circular plate structures with peripheral surface crack, *Journal of Sound and Vibration* 276 (3–5) (2004) 1081–1091.
[15] W. Flügge, *Stress in Shells*, Springer, Berlin, New York, 1973.
[16] C.R. Fuller, Effects of wall discontinuities on the propagation of flexural waves in cylindrical shells, *Journal of Sound and Vibration* 75 (2) (1981) 207–228.
[17] J.R. Rice, N. Levy, The part-through surface crack in an elastic plate, *Journal of Applied Mechanics* 3 (1972) 185–194.
[18] H. Tada, P.C. Paris, G.R. Irwin, *The Stress Analysis of Cracks Handbook*, Del Research Corporation, Hellertown, Pennsylvania, 1973.
[19] C.R. Fuller, Input mobility of an infinite circular cylindrical elastic shell filled with fluid, *Journal of Sound and Vibration* 87 (3) (1983) 409–427.

[20] J.W. Verheij, Measurements of structure-borne wave intensity on lightly damped pipes, *Noise Control Engineering Journal* 35 (2) (1990) 69–76.
[21] G. Pavic, Vibrational energy flow in elastic circular cylindrical shells, *Journal of Sound and Vibration* 142 (2) (1990) 293–310.
[22] A.R. Briscoe, R.J. Pinnington, Axisymmetric vibrational power measurement in empty and fluid filled pipes, *Journal of Sound and Vibration* 192 (4) (1996) 771–791.
[23] R. Ming, J. Pan, M.P. Norton, The measurement of structural mobilities of a circular cylindrical shell, *Journal of the Acoustical Society of America* 107 (3) (2000) 1374–1382.
[24] R.S. Ming, J. Pan, M.P. Norton, The measurement of structure-borne sound energy flow in an elastic cylindrical shell, *Journal of Sound and Vibration* 242 (4) (2001) 719–735.